Crystal structure and redox properties of a novel cyanobacterial heme protein with a His/Cys heme axial ligation and a Per-Arnt-Sim (PAS)-like domain

Received for publication, June 30, 2016, and in revised form, April 17, 2017 Published, Papers in Press, April 20, 2017, DOI 10.1074/jbc.M116.746263

Taiki Motomura[‡§1], Michihiro Suga[§1], Rainer Hienerwadel[¶], Akiko Nakagawa[§‖], Thanh-Lan Lai[**], Wolfgang Nitschke[‡‡], Takahiro Kuma[§], Miwa Sugiura[‖], Alain Boussac[**], and Jian-Ren Shen[‡§2]

From the [‡]Department of Picobiology, Graduate School of Life Science, University of Hyogo, Hyogo 678-1297, Japan, the [§]Research Institute for Interdisciplinary Science and Graduate School of Natural Science and Technology, Okayama University, Okayama 700-8530, Japan, the [¶]Laboratoire de Génétique et Biophysique des Plantes, UMR 7265, CNRS-CEA-Aix-Marseille Université, Faculté des Sciences de Luminy, 13288 Marseille, France, the [‖]Proteo-Science Research Center, Ehime University, Ehime 790-8577, Japan, [**]iBiTec-S, SB2SM, CNRS UMR 9198, CEA Saclay, 91191 Gif-sur-Yvette, France, and the [‡‡]Laboratoire de Bioénergétique et Ingénierie des Protéines, CNRS UMR 7281, 13402 Marseille Cedex 20, France

Edited by Joseph Jez

Photosystem II catalyzes light-induced water oxidation leading to the generation of dioxygen indispensable for sustaining aerobic life on Earth. The Photosystem II reaction center is composed of D1 and D2 proteins encoded by *psbA* and *psbD* genes, respectively. In cyanobacteria, different *psbA* genes are present in the genome. The thermophilic cyanobacterium *Thermosynechococcus elongatus* contains three *psbA* genes: *psbA1*, *psbA2*, and *psbA3*, and a new *c*-type heme protein, Tll0287, was found to be expressed in a strain expressing the *psbA2* gene only, but the structure and function of Tll0287 are unknown. Here we solved the crystal structure of Tll0287 at a 2.0 Å resolution. The overall structure of Tll0287 was found to be similar to some kinases and sensor proteins with a Per-Arnt-Sim-like domain rather than to other *c*-type cytochromes. The fifth and sixth axial ligands for the heme were Cys and His, instead of the His/Met or His/His ligand pairs observed for most of the *c*-type hemes. The redox potential, $E_{1/2}$, of Tll0287 was −255 ± 20 mV *versus* normal hydrogen electrode at pH values above 7.5. Below this pH value, the $E_{1/2}$ increased by ≈57 mV/pH unit at 15 °C, suggesting the involvement of a protonatable group with a pK_{red} = 7.2 ± 0.3. Possible functions of Tll0287 as a redox sensor under microaerobic conditions or a cytochrome subunit of an H_2S-oxidizing system are discussed in view of the environmental conditions in which *psbA2* is expressed, as well as phylogenetic analysis, structural, and sequence homologies.

This work was supported by a program for Leading Graduate Schools, "Next Generation Picobiology Pioneered by Photon Sciences" at the University of Hyogo, a program for promoting the enhancement of research universities at Okayama University; KAKENHI Grants JP24000018 (to J.-R. S.) and JP26840023, JP15H01642, JP16H06162, and JP16H06296 (to M. Suga) from Japan Society for the Promotion of Science; an Inamori Foundation grant (to M. Suga); Japan Science and Technology Agency (JST)-PRESTO Program 4018 (to M. Sugiura); and the Bioenergy Program of CEA-DSV (to T.-L. L. and A. B.). The authors declare that they have no conflicts of interest with the contents of this article.

The atomic coordinates and structure factors (code 5B82) have been deposited in the Protein Data Bank (http://wwpdb.org/).

This article contains supplemental Table S1 and Figs. S1–S4.

[1] These authors contributed equally to this work.

[2] To whom correspondence should be addressed. E-mail: shen@cc.okayama-u.ac.jp.

Photosystem II (PSII)[3] catalyzes the first photochemical reaction in oxygenic photosynthesis, leading to the splitting of water into electrons, protons, and dioxygen. In this way, PSII sustains oxygenic life on Earth by providing oxygen and converting light energy into biologically useful chemical energy. The central part of PSII is largely conserved from prokaryotic cyanobacteria to eukaryotic higher plants, and a typical PSII core from cyanobacteria consists of 17 transmembrane subunits and 3 peripheral, membrane-extrinsic subunits, with an overall molecular mass of ≈350 kDa for a PSII monomer. PSII exists in a dimeric form, and the structure of cyanobacterial PSII dimer has been solved up to 1.9 Å resolution (1, 2). The core of PSII is formed by two subunits, D1 and D2, which bind all the co-factors involved in the PSII electron transfer chain and are surrounded by two large chlorophyll protein subunits CP47 and CP43 (3–5).

The D1 protein is encoded by the *psbA* gene, which exists in a single copy in higher plants but in multiple forms in cyanobacteria (6). The isoforms of the D1 protein encoded by these different *psbA* genes in cyanobacteria have been reported to be differently expressed in response to various environmental conditions such as light intensity (7–9), the presence of UV-B (10, 11), chilling stress (12), reductive stress (13), and low O_2 (14) or microaerobic conditions (15, 16).

In the thermophilic cyanobacterium *Thermosynechococcus elongatus*, three homologous genes, *psbA1*, *psbA2*, and *psbA3*, are present in the genome (17). The PsbA1, PsbA2, and PsbA3 D1 proteins encoded by the *psbA1*, *psbA2*, and *psbA3* genes are expressed under different environmental conditions (15, 16, 18, 19). Of the 344 amino acid residues, 31 differ between PsbA1 and PsbA2, 21 differ between PsbA1 and PsbA3, and 27 differ between PsbA2 and PsbA3 (see Refs. 20 and 21 for reviews).

[3] The abbreviations used are: PSII, Photosystem II; CAPS, *N*-cyclohexyl-3-aminopropanesulfonic acid; β-DDM, *n*-dodecyl-β-maltoside; LDAO, *N*,*N*-dimethyldodecylamine *N*-oxide; NHE, normal hydrogen electrode; PDC, PhoQ-DcuS-CitA; PAS, Per-Arnt-Sim; SQR, sulfide:quinone-oxidoreductase; RMSD, root-mean square deviation; CBB, Coomassie Brilliant Blue; cyt, cytochrome; PDB, Protein Data Bank.

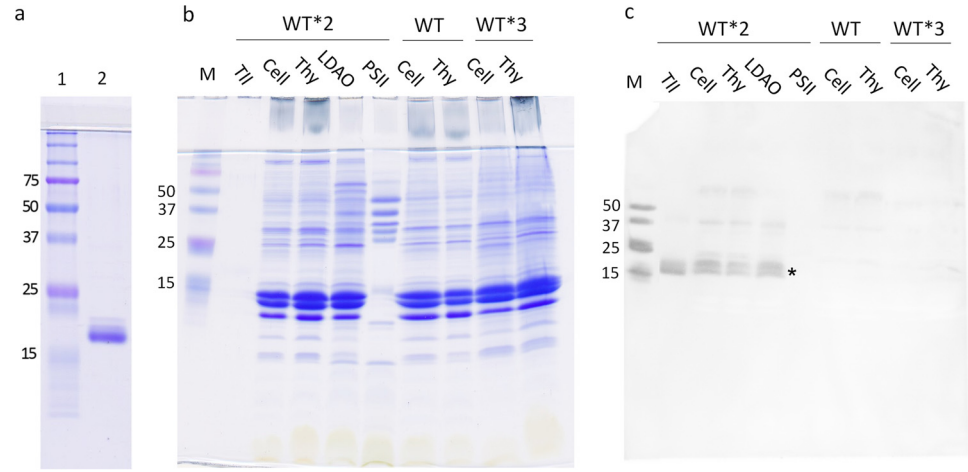

Figure 1. Immunoblot analysis on the expression and location of Tll0287. *a*, SDS-PAGE analysis with a 16% acrylamide gel of the purified Tll0287 protein (*lane 2*) used in this study. The molecular mass markers are shown in *lane 1*, with their molecular masses (kDa) indicated. *b*, CBB-stained gel of the samples used for immunoblot analysis shown in *c*. The samples shown are the purified Tll0287 protein (*Tll*), whole cell, and thylakoid fractions from the WT (predominately expressing *psbA1*), WT*2 (expressing *psbA2* only), and WT*3 (expressing *psbA3* only) strains, and crude-PSII (LDAO-PSII), PSII core complex purified from the *psbA*$_2$-expressing strain (WT*2). The amount of proteins loaded for each lane is equivalent to 2 μg of chlorophyll for the whole cell fractions and thylakoid membranes, 1 μg of chlorophyll for LDAO-PSII, 0.5 μg for purified PSII, and 0.16 mg of protein for the Tll0287 protein. *M* stands for molecular marker with the molecular masses indicated (kDa). *c*, immunoblot analysis with an anti-Tll0287 antibody for same samples shown in *b*.

In *T. elongatus*, some of the properties of PSII were found to be different depending on the *psbA* gene product (20, 21). For example, whereas the O_2-evolving activity was found to be similar in PsbA1- and PsbA2-containing PSII (PsbA1-PSII and PsbA2-PSII) (22), the PsbA3-containing PSII (PsbA3-PSII) had a higher O_2 evolution activity (23, 24). The redox potential of pheophytin, Q_A (primary quinone electron acceptor) and Q_B (secondary quinone electron acceptor), and the binding properties of some herbicides were also reported to be different in PsbA1-PSII and PsbA3-PSII (25, 26). On the other hand, the differences between PsbA2-PSII and PsbA1/A3-PSII are less documented. The structures of PsbA2-PSII and PsbA3-PSII have not yet been reported. However, a previous work showed that the geometry of the phenol group of Tyrz (redox-active tyrosine on the D1 subunit (D1-Tyr^{161}) in Photosystem II) and its environment, likely the hydrogen bond between Tyrz and D1/His^{190}, is modified in PsbA2-PSII in comparison with PsbA1/A3-PSII (22, 24).

Interestingly, a new EPR signal was detected in whole cells expressing the *psbA2* gene only (27). This EPR signal was identified to be originated from a hemoprotein that is the product of *tll0287*, a hypothetical gene encoding a ~19-kDa protein (consisting of 191 residues) with an unknown function (27). Genes homologous to *tll0287* are also found in several cyanobacteria (see "Discussion"). The amino acid sequence of the Tll0287 protein has a *CXXCH* motif characteristic for *c*-type cytochromes. Four different N-terminal sequences were detected for the mature Tll0287, suggesting multiple processing sites. In the present work, we purified the Tll0287 protein, solved its crystal structure, determined its midpoint potential, and investigated its cellular localization by immunoblot analysis. Possible functions of Tll0287 are discussed based on the sequence and structural homologies with other known proteins.

Results

Expression and location of the Tll0287 protein

The previous study has detected the novel EPR signal ascribed to Tll0287 in both soluble and membrane fractions from the *psbA2*-expressing cells but in neither the *psbA1*- nor the *psbA*$_3$-expressing cells (27). To confirm the different expression of Tll0287 in these three different strains, we used an anti-Tll0287 antibody. Fig. 1*a* shows an SDS-PAGE analysis of the purified Tll0287 protein used in this study, and Fig. 1*c* shows an immunoblot analysis with the anti-Tll0287 antibody in the whole cell and thylakoid fractions from WT (expressing mainly the *psbA1* gene), WT*2 (expressing the *psbA2* gene only), and WT*3 (expressing the *psbA3* gene only) strains. The amount of proteins loaded in each lane of Fig. 1*c* are shown in Fig. 1*b*, where exactly the same amount of the samples were loaded in each lane as in Fig. 1*c*. The results in Fig. 1*c* clearly show that Tll0287 is expressed in the WT*2 strain but is expressed little or not at all in the WT and WT*3 strains. In the immunoblots of the purified Tll0287 protein and various subcellular fractions from the WT*2 strain, weak bands at twice and four times the molecular mass of Tll0287 were detected, which may correspond to the non-native oligomeric form of Tll0287 that would be present even under SDS-PAGE conditions in a very low amounts. It should be noted that in *lane 2* (labeled *Tll* in Fig. 1*b*), the CBB-stained Tll0287 is barely visible, which is required to ensure that the immunoblot in Fig. 1*c* does not become too dense.

Tll0287 was also detected in a crude-PSII fraction (PSII purified with LDAO) from the WT*2 strain but not in purified PSII after extensive purification procedures involving two different detergents (LDAO and β-DDM) (Fig. 1*c*). The previous result has suggested that Tll0287 is co-purified with a His-tagged PSII (27); however, the PSII used in the previous study was obtained with a simple step of purification employing a mild detergent-

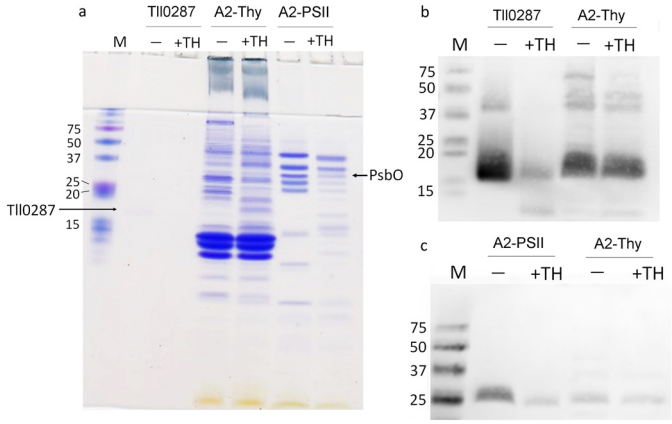

Figure 2. Digestion of the Tll0287 protein with a protease thermolysin. *a*, CBB-stained gel of the samples used for immunoblot analysis shown in *b* and *c*. The samples used are the purified Tll0287 protein, thylakoid membrane fraction from the WT*2 strain (A2-Thy, expressing *psbA2* only), and purified PSII from WT*2 (A2-PSII). The amount of the samples loaded on each lane was the same as that in Fig. 1*b*. *b*, immunoblot analysis of the Tll0287 protein in the purified Tll0287 sample and thylakoid membrane fraction (A2-Thy) from the WT*2 strain with an anti-Tll0287 antibody, either before (labeled −) or after digestion of the samples with 5 μg/ml thermolysin for 6 h (labeled +*TH*). *c*, immunoblot analysis of the PsbO protein in the purified PSII and thylakoid membrane fraction from the WT*2 strain with an anti-PsbO antibody, before (−) or after digestion of the samples with thermolysin (+*TH*) at the same conditions as for Tll0287.

solubilization and nickel affinity column. The present results therefore suggest that Tll0287 is likely not bound to PSII specifically. However, it should be noted that cyt *c*-550, an extrinsic protein associated with PSII rather strongly can also be dissociated from PsbA2-PSII, but not from PsbA1-PSII and PsbA3-PSII, during a size-exclusion chromatography performed under high pressure (results not shown), implying that it is sometimes difficult to conclude whether the binding of non-membrane proteins is real or not based on the co-purification only.

Although previous studies (27) have suggested the possible presence of Tll0287 at the lumenal side of the thylakoid membrane, its location remained to be confirmed. Therefore, the thylakoid fraction from the *psbA2*-expressing strain was treated with the protease thermolysin, together with the purified Tll0287 as a control, and the protease-treated samples were probed by immunoblot analysis (Fig. 2). The amounts of the samples loaded in each lane for the immunoblot analysis are shown in Fig. 2*a*, where again the band of purified Tll0287 was barely visible by CBB staining. Although the purified Tll0287 is largely digested by thermolysin, it was poorly digested by the protease in the thylakoid fraction (Fig. 2*b*). The exact situation was found for the PsbO protein (Fig. 2*c*), which has a well established lumenal location. The CBB-stained gel (Fig. 2*b*) showed that many bands were weakened in the thermolysin-treated thylakoid membrane fraction as well as the purified PSII, indicating the effective digestion by the protease. These results suggest that at least part of Tll0287 is located in the lumen of the thylakoid or periplasm if we consider that there may be some contamination of cytoplasmic membranes in the thylakoid membrane fraction used in the present study.

Determination of the midpoint potential of Tll0287

The redox titration of Tll0287 is shown in Fig. 3. *Panels a* and *b* in Fig. 3 show the absorption spectra recorded in the oxidative way and reductive way, respectively. The presence of well defined isosbestic points in the two panels shows that the protein was fully stable in these experimental conditions. Fig. 3*c* shows a Nernst plot for an oxidation (*blue points*) and a reduction (*red points*) titration performed at pH 8.5. The *continuous black line* is a global fit with $n = 1$ and $E_{½}' = -255 \pm 20$ mV *versus* NHE. Finally, Fig. 3*d* shows the pH dependence of the $E_{½}'$ determined as above at different pH values (the data points are from electrochemical experiments performed on Tll0287 from three batches). The continuous line is the result of a fitting procedure with the following equation: $E_{½}' = E_0' - 57 \log((K_{ox} + [H^+])/(K_{red} + [H^+]))$, where E_0' is the midpoint redox potential of the fully protonated form, and K_{red} and K_{ox} are the ionization constants of the protonatable group when the iron is reduced and oxidized, respectively (28). The E_0' value was found to be -255 ± 20 mV *versus* NHE at pH values above p$K_{red} = 7.2$, and the pK_{ox} value was ≤5.5.

Structure determination

Tll0287 was purified from the pool of non-membrane proteins, and crystals of the isolated protein were grown at 20 °C for a few days. The crystals appeared as red needles with a maximum size of 0.4 × 0.02 × 0.02 mm. The crystals belong to the space group $P4_22_12$ with unit cell dimensions $a = b = 101.2$ Å, $c = 33.1$ Å (Table 1). Phase information was obtained by the single-wavelength anomalous diffraction method using anomalous diffraction from the iron ion of the heme, and the model was refined to a resolution of 2.0 Å with R_{factor} and R_{free} values of 0.1765 and 0.2336, respectively.

The structure of Tll0287 is shown in Fig. 4*a*. It contains residues 26–186 (the full length of the protein is 191 residues), a heme *c*, a tentatively assigned chloride ion, and 84 water molecules. The secondary structure of the domain was defined as follows: α-helices, α1: 28–49, α2: 68–82, α3: 103–114, α4: 139–146, and α5: 153–158; β-strands, β1: 85–89, β2: 120–125, β3: 128–136, and β4: 172–181. The helix α2 is antiparallel to the N-terminal end of helix α1. The β-strands are arranged in an antiparallel fashion and surrounded by three α-helices α1, α2, and α3.

Fig. 4*b* shows the surface charge distribution of Tll0287. The periphery of the heme ligand is relatively positive (Fig. 4*c*), and a concave pocket was found between the four β-strands bundle and α3 (Fig. 4*b*), which is also apparent in the overall structure of Tll0287. Fig. 4*d* shows that Tll0287 indeed exhibits a large hydrophobic surface as predicted from the properties observed during its purification (27).

MALDI-TOF/MS analysis of the Tll0287 protein before crystallization detected peaks at *m*/*z* values of 18,633, 18,997, 19,162, 19,858, and 20,382 (Table 2). The peak at *m*/*z* 19,162 Da is equal to the molecular mass of the Tll0287 peptide with 24 residues truncated at the N-terminal region (Δ24) and with the heme bound (27). The other fragments may correspond to Tll0287 truncated at 11 or 12, 17, and 26. Because the previous study showed that the Δ24 fraction likely dominates the heme-bound form of Tll0287 (27), our heme-containing structure likely corresponds to the Δ24-truncated protein. This is also in agreement with the sequence analysis by SignalP, which suggested that this protein possesses a signal peptide that cleaves between 24 and 25 residues. The mass analysis, however, did

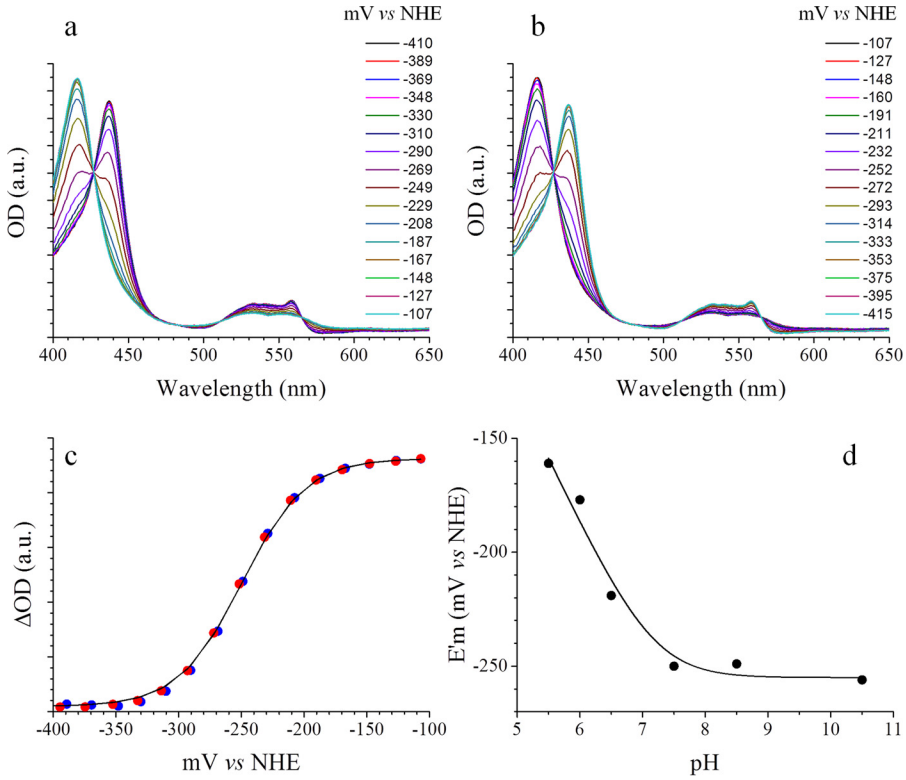

Figure 3. Electrochemistry on Tll0287. *a* and *b* show the absorption spectra recorded at the indicated potential during the oxidative and reductive processes, respectively. *c* shows a Nernst plot for an oxidation (*blue points*) and a reduction (*red points*) performed at pH 8.5 and $T = 15$ °C. The *continuous black line* is a global fit with *n* fixed to 1 and $E_{1/2}' = -255$ mV *versus* NHE. *d* shows the pH dependence of the $E_{1/2}'$ determined as above at different pH values. The *continuous line* is the result of a fitting procedure with the following equation: $E_{1/2}' = E_0' - 57\log((K_{ox} + [H^+])/(K_{red} + [H^+]))$, where E_0' is the midpoint redox potential of the fully protonated form, and K_{red} and K_{ox} are the ionization constants of the protonatable group when the iron is reduced and oxidized, respectively. The pK_{red} was found to be 7.2.

Table 1
Data collection and structural refinement statistics

	Native	Iron peak
Data collection		
Wavelength	0.900	1.730
Space group	$P4_22_12$	$P4_22_12$
Unit cell	$a = b = 101.2$ Å, $c = 33.1$ Å, $\alpha = \beta = \gamma = 90.00°$	$a = b = 100.9$ Å, $c = 33.1$ Å, $\alpha = \beta = \gamma = 90.00°$
Resolution (Å)	20–2.00 (2.13–2.00)[a]	20–3.20 (3.39–3.20)
Unique reflections	12,169 (2,047)	5,410 (856)
Redundancy	12.7 (12.9)	25.0 (13.8)
Completeness	100.0 (100.0)	99.6 (97.5)
R_{merge}[b]	10.2 (95.5)	8.8 (21.9)
$I/\sigma(I)$	19.1 (2.8)	36.5 (10.9)
R_{means} (%)[c]	10.6 (99.4)	9.0 (22.7)
$CC_{1/2}$[d]	99.9 (96.8)	99.9 (99.0)
Structural refinement		
R_{factor}	0.1765	
R_{free}	0.2336	
Number of atoms	1,422	
Proteins	1,294	
Ligands	44	
Water	84	
Number of residues	161	
RMSD		
Bond	0.007	
Angle	1.030	
Average B-factor	36.1	
Ramachandran plot[e]		
Favored (%)	99.4	
Allowed (%)	0.6	
Outliers (%)	0.0	

[a] Statistics for the highest resolution shell are shown in parentheses.
[b] $R_{merge} = \Sigma_{hkl}\Sigma_i|I_i(hkl) - <I(hkl)>|/\Sigma_{hkl}\Sigma_i I_i(hkl)$, where $I_i(hkl)$ is the intensity of the reflection, and $<I(hkl)>$ is the mean intensity of a group equivalent reflection.
[c] *R* factor independent of the redundancy.
[d] Percentage of correlation between intensities from two random half-data sets.
[e] Calculated with the MolProbity (see "Experimental Procedures").

not give information regarding the relative ratio of other fragments in the purified Tll0287 protein solution.

Heme in the Tll0287 protein

The fifth and sixth heme iron axial ligands are Cys^{68} and His^{145} (Fig. 4*c*); this is remarkably different from most of the *c*-type cytochromes in which His/Met or His/His axial ligands are found. It also appears that the Cys^{68} axial ligand is close to Arg^{45} and may be stabilized by it, whereas the His^{145} axial ligand is supported by the carbonyl group of Ala^{164} and is also close to Arg^{94} and Arg^{173}.

Expression level of the Tll0287 protein in the dark

As mentioned in the Introduction, the expression level of *psbA2* was reported to increase under microaerobic conditions (14–16), and as discussed under "Discussion", in *Synechocystis sp.* PCC6803 it has been shown that *sll5034* (analogous to *tll0287*) was transcribed at a higher level in the dark, an environment possibly comparable to microaerobic conditions (29). We have therefore compared the level of expression of Tll0287 between the whole cells of WT, which mainly express *psbA1*, with those of WT*2 cells, under different light conditions. Fig. 5 shows the EPR spectra recorded from WT and WT*2 cells cultivated under either normal light conditions (*i.e.* 120 μE m^{-2} s^{-1}) or after a further dark period of 3–4 h. The magnetic field region shown allows us to compare the relative amplitude of three resonance signals, namely, the Fe^{3+} superoxide dismutase signal labeled with an *asterisk* between 1300 and 2000 gauss

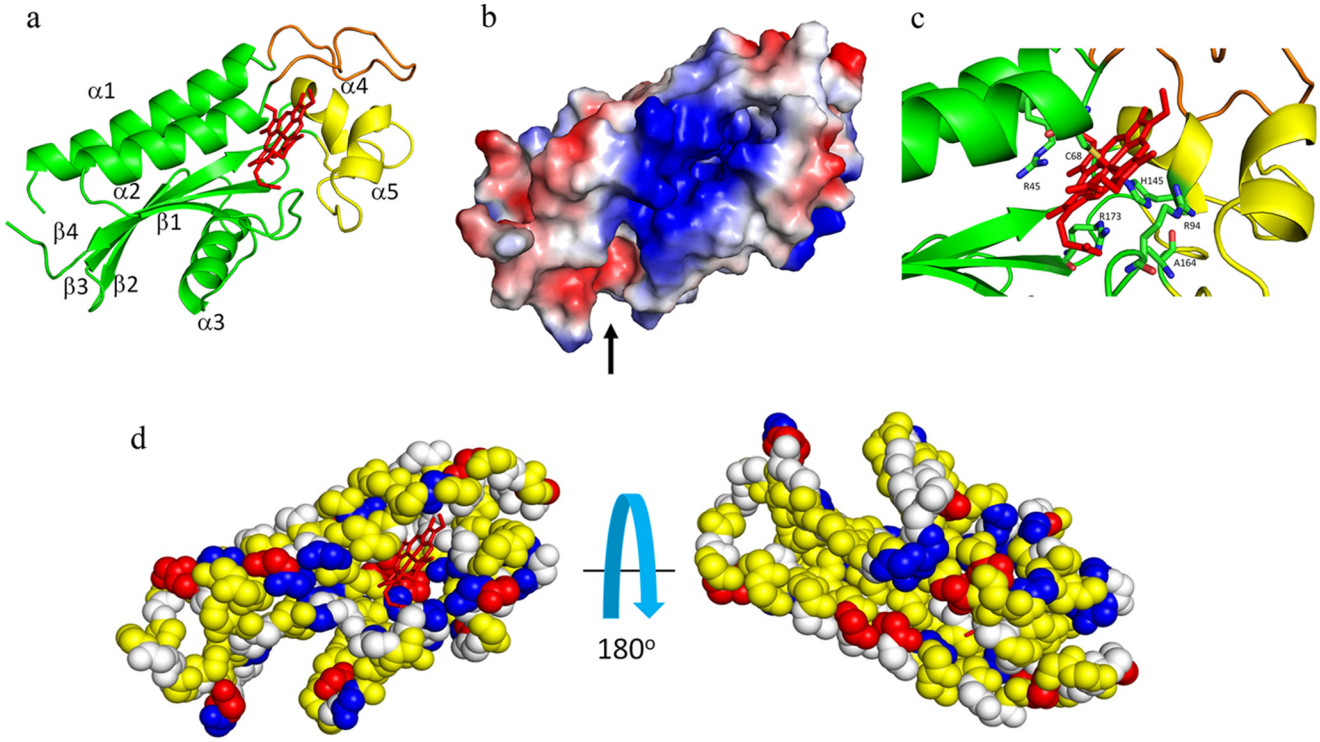

Figure 4. Crystal structure of the Tll0287 protein. *a*, overall structure of the Tll0287 protein. The PAS-like domain composed of three α-helices and four β-strands is depicted in *green*; the heme and its binding part are depicted in *red* and *yellow*, respectively; and the loop region is depicted in *orange*. *b*, surface charge distribution of the Tll0287 protein. *Blue* and *red* represent negative and positive areas, respectively. The area surrounding the heme is largely positive. The *black arrow* indicates a concave pocket. *c*, ligand environment of the heme *c* in Tll0287. The fifth and sixth heme iron axial ligands, Cys^{68} and His^{145}, and the residues around them are depicted in stick models. *d*, hydrophobicity characters of the surface of Tll0287. The structure of Tll0287 was depicted in a ball model in the same direction (*left side*) as that in panels *a* and *b*, and in a direction rotated 180° (*right side*). *Blue* represents positively charged residues (Arg, Lys, and His), *red* represents negatively charged residues (Asp and Glu), *white* represents hydrophilic residues, and *yellow* represents hydrophobic residues.

Table 2
Experimentally determined by MALDI-TOF/MS and calculated molecular masses of Tll0287

Experimentally measured mass (Da) $[M + H]^+$	Calculated mass (Da) $[M + H]^+$		Processing site	N-terminal sequence
	− Heme	+ Heme		
20,382	19,838.16	20,456.37	11/12 (Δ11)	ASLWI[a]
20,382	19,767.08	20,351.28	12/13 (Δ12)	SLWIQ[a]
19,858	19,139.35	19,757.56	17/18 (Δ17)	GSPAP[a]
18,633 or 19,162	18,545.68	19,163.89	24/25 (Δ24)	SANPE[a]
18,997	18,387.52	18,969.03	26/27 (Δ26)	NPEEL[a]

[a] N-terminal sequence found with the Edman procedure in previous research (27).

(30), the g_z resonance of the soluble fraction of cyt *c*-550 labeled with an *asterisk* between 2200 and 2300 gauss (31), and the g_z resonance of Tll0287 labeled with an *asterisk* at ~2800 gauss (27). The large signal from Mn^{2+} present in the cells precluded the detection of resonances other than cytochromes. The data in Fig. 5 clearly show that although the g_z resonance signal of Tll0287 was virtually not detected in the WT cells grown either under normal light conditions (spectrum *a*) or after a further dark period (spectrum *b*), the level of expression of Tll0287 was approximately doubled upon a short dark period in the WT*2 cells when compared with other EPR detectable proteins (spectra *c* and *d*).

Discussion

Location, structure, and physical chemical properties of Tll0287

The present results confirmed that the Tll0287 protein is highly expressed in a strain expressing *psbA2* but not in the WT (expressing predominantly *psbA1*) and WT*3 (expressing only *psbA3*) strains. Furthermore, it is shown that this protein is likely located in the thylakoid lumen and/or in the periplasm based on the protease digestion results. This location is in agreement with sequence analysis by SignalP, which suggested that this protein possesses a cleavage site between residues 24 and 25 (not shown). The lumenal or periplasmic location is also consistent with the structural analysis showing that this protein has a globally similar structure to the PhoQ-DcuS-CitA (PDC) domain of some proteins involved in signal transduction with a periplasmic PAS fold instead of a cytoplasmic one (see "Sequence and structure similarity"). However, we cannot exclude the possibility that another fraction of the Tll0287 protein may be located in the cytoplasm. This would be consistent with the results of MS analysis showing that the purified protein had several N termini (27) consistent with different cleavage sites. Thus, it is possible that the protein has a dual location and possibly multiple functions. Interestingly, three other possible cleavage sites at the N-terminal region are also predicted by

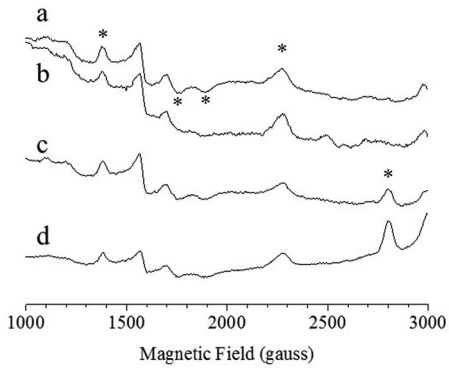

Figure 5. Expression level of Tll0287 under dark conditions. *Spectrum a*, WT whole cells cultivated for 2 days under normal light conditions. *Spectrum b*, WT whole cells after a further dark period of 3–4 h. *Spectrum c*, WT*2 whole cells cultivated for 2 days under normal light conditions. *Spectrum d*, WT*2 whole cells after a further dark period of 3–4 h. For sake of comparison, the spectra were approximately scaled by using both the Fe^{3+}SOD signals (labeled with *asterisk* between 1300 and 2000 gausses) and the g_z signal of cyt *c*-550 (labeled with *asterisk* between 2200 and 2300 gausses). The signal from Tll0287 is located at ~2800 gauss. Instrument settings were as follows: modulation amplitude, 25 G; microwave power, 5 milliwatts; temperature, 20 K; microwave frequency, 9.4 GHz; and modulation frequency, 100 kHz.

SignalP, but with a lower probability. These predicted sites correspond to the other N-terminal sequences found for Tll0287, although in these cases probably no heme is incorporated (27). Further studies are required to understand these observations.

The crystal structure of Tll0287 showed that the heme has a His/Cys ligation pattern, which is distinctly different from the typical His/Met or His/His ligand pairs for most of the *c*-type cytochromes. Such *c*-type heme with His/Cys axial ligation generally has a lower midpoint potential, typically below −400 mV, than other cytochromes with either a His/His or a His/Met axial coordination (32–36). Here, the midpoint potential of Tll0287 was determined to be −255 ± 20 mV *versus* NHE at pH 8.5 and to be pH-dependent involving a protonatable group with a p*K* at 7.2 ± 0.3 in the reduced state. The nature of this group is under investigation by using vibrational spectroscopy.

The His/Cys ligation pattern for the heme in Tll0287 is the second one found in cyanobacteria. The first one is PsbV2 (37), a *c*-type heme protein similar to PsbV (*i.e.* the cyt *c*-550), but with unknown function, although it has been reported that this protein may partially support the photoautrophic growth of *Synechocystis* 6803 in place of the PsbV protein (38). Fig. 6*a* shows the superimposition of the structure of Tll0287 with that of PsbV2. Surprisingly, although the heme structures can be superimposed with a root-mean square deviation (RMSD) of 0.8 Å, the overall structures of the two proteins are remarkably different. Because the structure of PsbV2 belongs to the general folding of *c*-type cytochromes and is rather similar to other *c*-type cytochromes (37), the present results indicate that the structure of Tll0287 is different from those of typical *c*-type cytochromes.

The ligand pair of His/Cys is different from the His/Tyr ligand pair previously erroneously predicted from the EPR spectrum (27). Indeed, using the formalism developed in Ref. 39 (see also Ref. 40 for a review), the crystal field parameters such as the rhombicity (ν/Δ) and the tetragonality (Δ/λ) can be calculated from the g_z, g_y, and g_x values of the EPR signal. These structural parameters put Tll0287 in a domain close to the His/$TyrO^-$ domain (supplemental Fig. S1). From the EPR data available in the literature, the rhombicity and tetragonality parameters can now be calculated for at least 10 hemoproteins with a His/Cys axial ligation. With the exception of the *b*-type heme, the cystathionine β-synthase (41) and ATP-dependent potassium channels (42), the *c*-type heme PsbV2 (37), DsrJ (32), NaxLS (33), triheme in *Rhodovulum sulfidophilum* (35), SoxAX (34), cyt c_6 M58C (43), RcoM 2 (44), and cyt *c* T58C/L79G/M80X mutant (45) are very close to each other and at the interface of three other domains already identified (supplemental Fig. S1). In contrast, Tll0287 is slightly outside of this small domain. This at least shows that such a graph can only be indicative mainly when it concerns hemoproteins having a structure largely different from the others, as mentioned above. Construction of a cyt *c*-550 mutant with His/Cys axial ligation has been reported in *T. elongatus* (46). However, cyt *c*-550 purified from this mutated strain had the same EPR signals and redox potential as that of the WT cyt *c*-550, which strongly suggests that the construction failed in obtaining a His/Cys cyt *c*-550 mutant.

Sequence and structure similarity

Because the structure of Tll0287 is unique in that it does not resemble those of the typical *c*-type cytochromes, we searched for possible similar structures with the DALI server (47). The results (supplemental Table S1) showed that the structure of Tll0287 is similar to that of a sensor domain contained in some kinases or sensor proteins possibly involved in cellular signal transduction, such as the sporulation kinase *d* domain from *Bacillus subtilis* (KinD, PDB code 4JGO) (48) (Fig. 6*b*) and a methyl-accepting chemotaxis protein (Mcp, PDB code 3C8C) (Fig. 6*c*), even though they do not contain a heme. These proteins have a PAS-like domain, especially a PDC domain as extracellular sensors (49), although the RMSD values between the overall structures of Tll0287 and these proteins were ~2.2 and 3.2 Å, respectively. Fig. 7 shows the results of multiple structural alignments by the DALI server (47). It is clear that although the primary sequences of Tll0287 and other proteins are not similar, the secondary structures appear to exhibit significant similarities. On the basis of the comparisons of the secondary (Fig. 7) and three-dimensional structures (Fig. 6), the structure of Tll0287 can be divided into three domains: a PAS-like domain (Ala^{26}–Ala^{49}, Val^{67}–Gln^{138}, and Val^{169}–Ala^{181}), a heme binding site (Ala^{139}–Arg^{168}), and a loop domain (Ser^{50}–Ala^{66}) that separates the PAS-like and heme-binding domains.

PAS domains were discovered as the large regions of *per*, *arnt*, and *sim* genes in *Drosophila* (50, 51) that are related to circadian rhythmicity (52) and are signaling modules that monitor changes in the redox potential, light, oxygen level, small ligands, or overall energy level of the cell (53). So far, proteins with the PAS domain are found as transcription factors in clock genes (54), ion channels such as HERG (55), and sensor proteins such as kinases (53). The PAS domains are composed of a single antiparallel, five-stranded β-sheet with the strand order of 2-(1)-5–4-3 (some proteins have only four-stranded β-sheet without the first strand, such as the sensor domain of histidine

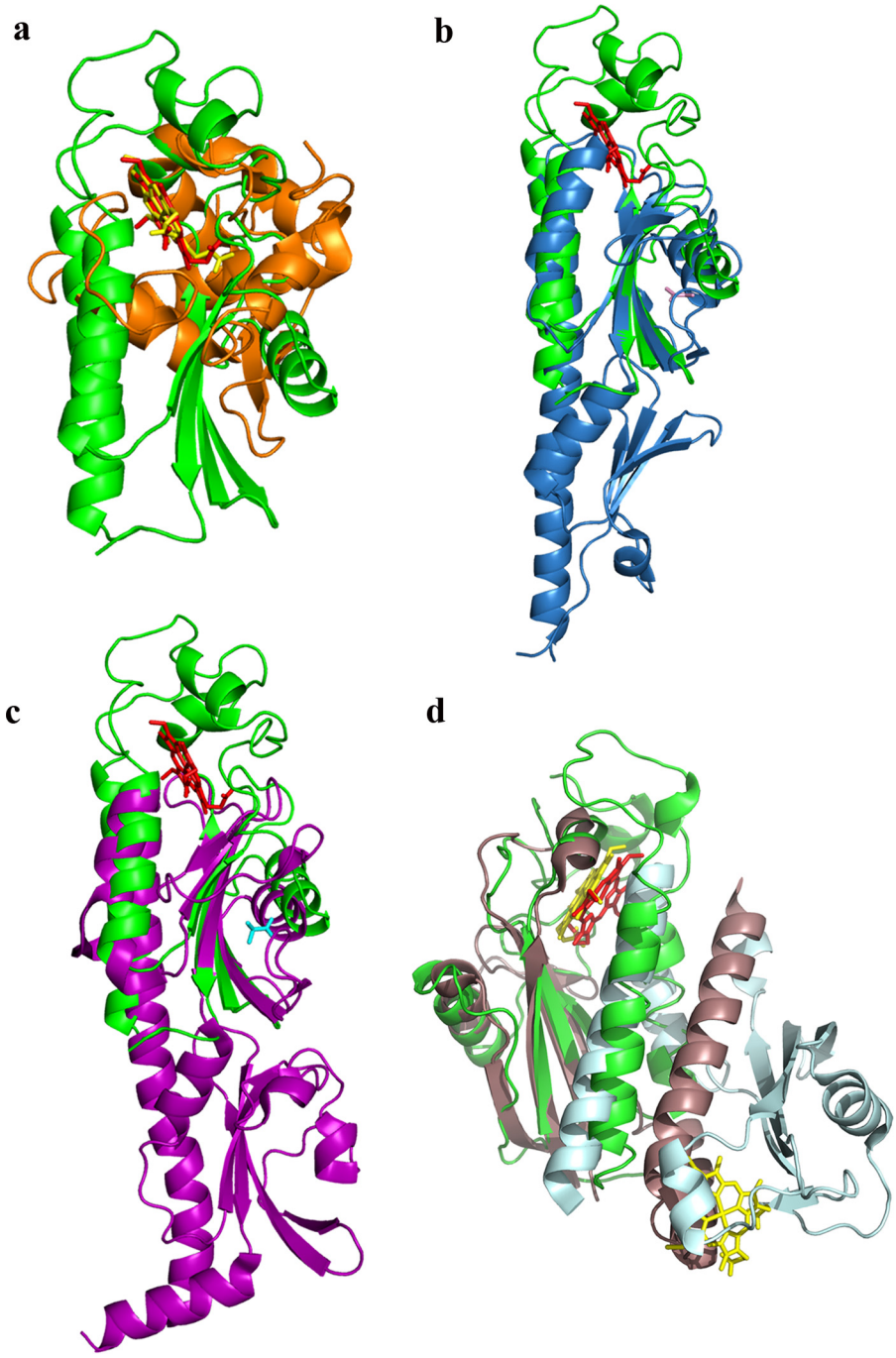

Figure 6. Structural comparison of the Tll0287 protein with other proteins. *a*, superposition of Tll0287 and PsbV2 from *T. elongatus* (PDB code 4LJI) (37). The colors for the Tll0287 protein and its heme are *green* and *red*, respectively, and those for the PsbV2 protein are as follows: heme, *yellow*; others, *orange*. *b*, superposition of Tll0287 and the sporulation kinase D sensor domain from *B. subtilis* (*blue*, A chain of PDB code 4JGO; *pink*, the ligand of this protein, pyruvate) (48). *c*, superimposition of Tll0287 and a methyl-accepting chemotaxis protein (Mcp) (*purple*, A chain of PDB code 3C8C; *cyan*, the ligand of this protein, alanine). *d*, superimposition of Tll0287 and the dimer of the non-membrane part of GSU0935 (PDB code 3B42) (62).

kinase DcuS (PDB code 3BY8)) (48) and several α-helices (56). Although the PAS domains have a conserved three-dimensional fold, these domains share little primary sequence identity (57). The homologous structure of Tll0287 revealed in this study is consistent with these features and suggests that Tll0287 also contains the PAS-like domain.

A subclass of the PAS domain is the PDC domain, which is a general feature of periplasmic PAS domains (58) and may bind multiple ligands (59). The periplasmic PAS domains typically contain three N-terminal helices, a central helical linker region, and a C-terminal α-helix, which are separated by two and three β-strands respectively, forming a 3α-2β-$1/2\alpha$-3β-1α arrangement. The secondary structure of the Δ24-truncated Tll0287 revealed by our present structural analysis was 2α-1β-1α-2β-2α-1β (Figs. 4*a* and 7). Considering the lack of the N-terminal region and the possible insertion of the α-helix in the heme binding site, it seems that Tll0287 is similar to the structure of the PDC domain, namely the periplasmic PAS domain, rather

Figure 7. Structural alignment of the Tll0287 protein with 11 homologous proteins. Eleven representative proteins are selected from supplemental Table S1 that show structural similarities with Tll0287, excluding their similar molecules. Inserted segments relative to the Tll0287 protein structure are hidden. The *upper part* shows the alignment of the amino acid sequence, and the *lower part* shows the secondary structure assignments performed by DSSP (65, 66). *H*, helix; *E*, strand; *L*, coil.

than the cytoplasmic PAS domain, which has a 1α-2β-4α-3β folding pattern (58).

Previous studies have suggested that the sensor domain of KinD has an extra ligand between the α-helix and β-strands, and the ligand binding site may accommodate small molecules related to metabolism such as pyruvate or propionate (48). In the electron density map of Tll0287, we indeed found an extra density at the similar position between the α-helix and β-strands (Fig. 8), which is in the concave pocket shown in Fig. 4. It seems that the extra density is surrounded by the guanidine group of Arg^{87} and the carboxyl group of Asp^{105} and Thr^{179}.

To identify the possible ligand corresponding to the extra density, we used the Arp/wARP program (60) for prediction of the extra ligand, which suggested that the extra ligand may be 2-oxoglutaric acid, although its abundance may be low in the thylakoid lumen. On the other hand, MALDI-TOF/MS measurements of the Tll0287 sample after trypsin digestion showed extra masses of 617, 74, and 118 Da (data not shown). The former two correspond to the masses of heme *c* and chlorine, respectively, whereas the mass of 118 Da has no corresponding molecules and may therefore be derived from the extra ligand. This mass is similar to those of homoserine, valeric acid such as norvaline, or betaine, which was used as an additive in the purification buffer. Although our current results do not allow the identification of the extra ligand, they suggest that Tll0287 has a PDC-like domain with an extra ligand.

The PAS-like domain found in the Tll0287 structure suggests that this protein may have a function in signal transduction or in response to some environmental factors. In relation to this, it is interesting to note that the expression level of *psbA2* is reported to increase under microaerobic conditions (14–16), and the EPR data in Fig. 5 show that under conditions in which

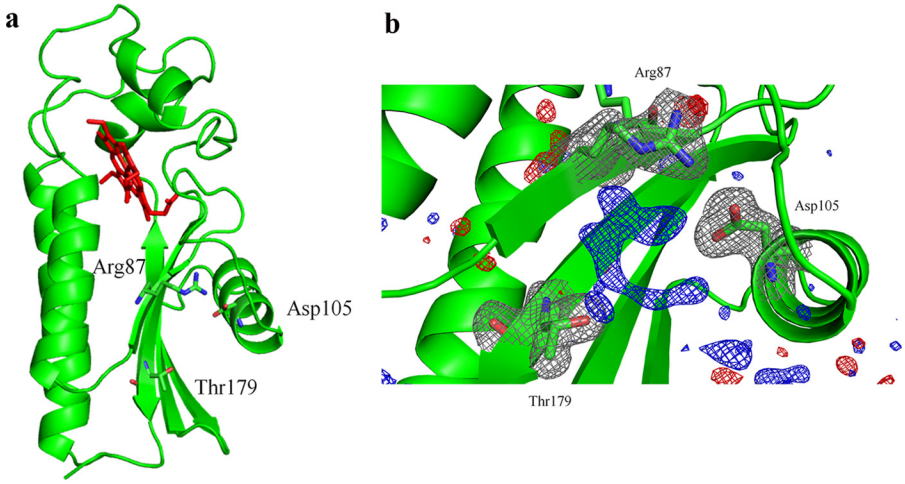

Figure 8. A possible extra ligand in Tll0287. *a*, the residues Arg[87], Asp[105], and Thr[179] surrounding the concave pocket (shown in Fig. 4*b*) are depicted as *stick models*. *b*, electron density map of a possible ligand corresponding to the ligand binding site in the structure of the sporulation kinase D sensor domain (48). The *blue mesh* and *red mesh* represent mF_o − DF_c omit map (positive and negative, respectively) contoured at 3.5 σ distributions, and the *gray mesh* represents 2mF_o − DF_c map contoured at 1.0 σ distributions.

O_2 was not produced, the expression level of Tll0287 increased in the WT*2 strain, at least transiently.

A second approach searching for structural similarities was done by using the Phyre[2] server (61), which revealed a good structural similarity with GSU0935, a methyl-accepting chemotaxis protein from *Geobacter sulfurreducens* (PDB code 3B42) (62) (Fig. 6*d*). This *b*-type heme protein also shows a PAS-type fold but exhibits axial ligations (His-water and His-Met) different from that of Tll0287 with a high-spin configuration in the oxidized state. The overexpressed non-membrane part of GSU0935 was crystallized as a dimer (62). Interestingly, as shown in Fig. 6*d*, the heme part of one monomer of GSU0935 fits very well with the heme part of Tll0287, and the two α-helices of the opposite monomer fit very well with two of the α-helices, α1 and α2 of Tll0287, although they do not have counterparts in the first monomer. Such similarities may suggest that, *in vivo*, Tll0287 is present as a dimer with a structure similar to the dimer of GSU0935.

These structurally similar proteins have a transmembrane region and active site in the C terminus after the PAS domain (48, 62), whereas Tll0287 has no region after the PAS domain. Instead, Tll0287 has a heme *c* inserted. It is possible that the heme *c* may sense some environmental conditions such as the oxygen level or redox state of the cell that may therefore induce structural changes of the heme. This structural change may be transmitted and/or enlarged through the PAS-like domain.

Tll0287 homologs, genomic context, and phylogeny

Homology sequences of Tll0287 were searched with BLAST for cyanobacteria, as well as non-cyanobacterial prokaryotes. Genes with substantial sequence homologies (BLAST search expectation values exceeding e-50, which is a corrected value of the probability that an event occurs by chance), in particular with the C-terminal *CXXCH* motif, were detected in several cyanobacteria but also outside the cyanobacterial phylum (supplemental Fig. S2). Although some of these non-cyanobacterial genes coded for larger, two-domain proteins that likely correspond to two-component sensors, others encoded monotopic cytochromes with sizes similar to that of Tll0287 (see phylogenetic tree in supplemental Fig. S3*A*). To glean insight into their functions, we compared the genomic context of all these Tll0287- and Tll0287-like genes. The following observations emerge: (*a*) no common features are obvious between cyanobacterial and non-cyanobacterial cases, and (*b*) in cyanobacteria, Tll0287-homologous genes occur almost exclusively in close genomic association with a gene coding for sulfide:quinone-oxidoreductase (SQR). The only exception to this rule is *Arthrospira platensis*, in which the Tll0287 homolog and the SQR genes are distantly positioned in the genome. It is noteworthy that the majority of these SQR genes are annotated as NDH-2 (type 2 NADH-dehydrogenase), but the phylogenetic analysis (supplemental Fig. S3*B*) clearly shows that they all cluster together with *bona fide* SQR from *Oscillatoria limnetica* (63) and not with NDH-2. Remarkably, the tree of SQR sequences retrieved from the cyanobacterial clade falls into two distinct subclades: one contains species in which SQR but not Tll0287-homologous genes are present, whereas in the second subclade, SQR genes co-occur with Tll0287 homologs. Two distinct scenarios can be proposed based on this pattern of co-occurrence: (*a*) the sulfide dehydrogenase in the clade where "SQR" and Tll0287 homologs co-occur is actually a sulfide:cytochrome-oxidoreductase rather than a sulfide:quinone-oxidoreductase, and the Tll0287 gene product would in fact correspond to the cytochrome subunit of an H_2S-oxidizing enzyme, reminiscent of so-called flavocytochrome *c*-sulfide dehydrogenase observed in a number of prokaryotes (64); and (*b*) the association of Tll0287-homologous genes to sulfide metabolism is more indirect and potentially even related to some kind of sensory mechanism (it could be noted here that several of the hemo proteins with His-Cys axial ligation are involved in the sulfide metabolism). We presently consider the first possibility as less likely because (*a*) no co-purification of Tll0287 and SQR has been observed so far, and (*b*) the sequence motif involved in forming the quinone-binding pocket in SQR (GQMTEE in

Caenorhabditis elegans, deduced from the three-dimensional structure of *Aquifex aeolicus* SQR; PDB code 3HYW) is highly conserved in both subclades arguing for true SQR-type functional characteristics of all enzymes in both clades. However, in *Synechocystis sp.* PCC6803, it has been shown that *sll5034* (analogous to *tll0287*) and the SQR (coded by *sll5036*) belong to the same operon and are indeed co-transcribed with a higher level of transcription in the dark, possibly equivalent to microaerobic conditions (29). Such a higher level of expression of Tll0287 in the dark was also observed in the WT*2 strain (Fig. 5), suggesting a role for this protein in sensing the environmental conditions. The actual functional significance of Tll0287-homologous genes in cyanobacteria therefore remains enigmatic, but an involvement in H_2S oxidation as studied in *O. limnetica* (63) represents an intriguing lead. In this context, it is noteworthy that, with the sole exception of *Pleurocapsa minor*, we only found Tll0287 homologs in members of the *Oscillatoriaceae*.

Experimental procedures

T. elongatus strain, cultivation of cells, and purification of the Tll0287 protein

The *T. elongatus* strain used in this work was the WT*2 strain in which a His tag was attached in the C terminus of CP43, and both *psbA1* and *psbA3* were deleted so that only *psbA2* was expressed for the D1 subunit (22, 27). The WT*3 strain that expresses the *psbA3* gene only was made as described (23). The cells were grown in 1-liter cultures of DTN medium with a CO_2-enriched atmosphere at 45 °C under continuous light (Grolux, Sylvania). The cells were collected by centrifugation (Beckman) with a JA10 rotor and were suspended in a buffer containing 100 mM NaCl, 10 mM Tris, pH 8.5, and 0.03% β-DDM, 1 mM benzamidine, 1 mM ϵ-aminocaproic acid, and DNase I, and disrupted by a French press. The Tll0287 protein was purified from the soluble proteins upon the breakage of the cells, *i.e.* after the removal of the membrane fraction by centrifugation based on the procedures described previously (27) with some modifications. The supernatant was concentrated and then loaded onto a gel filtration column (Sephadex 75, HiLoad 26/60). The buffer used for this column contained 100 mM NaCl, 10 mM Tris, pH 8.5, and 0.03% β-DDM, and the flow rate was 1 ml/min. The fraction of eluate containing Tll0287 (which was judged based on the approximate molecular masses eluted from the column and the reddish color of the heme together with the measurement of the absorption spectra taken every 4 ml) was collected and further purified with a Mono Q column (GE Healthcare) at pH 8.5 with a NaCl gradient in the presence of 0.03% β-DDM and a flow rate of 0.5 ml/min. Finally, the fraction eluted from the Mono Q column was diluted 3–5-fold and purified by a Mono S column (GE Healthcare) at pH 8.5 with a NaCl gradient in the presence of 0.03% β-DDM and a flow rate of 0.5 ml/min. In all cases, the fraction containing Tll0287 was easily followed by the color of the heme. Under the conditions used, Tll0287 was eluted from the Mono Q and Mono S columns with a gradient of 100–150 mM NaCl, but other proteins that are either more tightly or more loosely bound to the resins eluted differently from the two columns which allowed us to separate them efficiently. It should be noted that (*a*) the detergent was added in all of the purification steps to prevent almost irreversible binding of the protein to the resins and to hydrophobic surfaces because of the high hydrophobic character of Tll0287; and (*b*) hydrophobic resins like phenyl-Sepharose cannot be used because the protein binds almost irreversibly to such resins. Tll0287 was then concentrated using a Millipore Amicon Ultra-15 centrifugal filter devices with a cutoff value of 10 kDa. By comparing the relative contents of Tll0287 and soluble Cyt *c*-550 (*i.e.* the fraction of Cyt *c*-550 not bound to PSII easily identifiable by its EPR signal different from the PSII bound fraction) with EPR in whole cells before breakage and the amounts of Tll0287 and cyt *c*-550 purified in parallel from the same batch of the cells, the protocol described above allows the purification of a very large proportion of Tll0287 present in the cells.

Crystallization and X-ray data collection

Initial crystallization conditions were screened with an automatic dispensing machine (Mosquito, TTP Labtech) with over 800 commercially available screening conditions at a concentration of 2 mg protein/ml. One of these conditions composed of Na_2HPO_4, K_2HPO_4, $(NH_4)_2HPO_4$, and Tris, pH 8.5, produced small crystals with a red color of Tll0287. These small crystals were used as seeds to grow larger crystals under the same condition for 2 weeks at 20 °C. The crystals obtained were needle type, and they were cryo-protected using a solution containing 0.7 M Na_2HPO_4, 0.7 M K_2HPO_4, 0.1 M $(NH_4)_2HPO_4$, and 0.1 M Tris, pH 8.6, in either the presence or the absence of 25% (w/v) glycerol in a stepwise fashion, and flash frozen under liquid nitrogen gas. X-ray diffraction data were collected at Beamlines BL41XU and BL44XU of SPring-8 at a wavelength of 0.900 Å for a native data set and at 1.730 Å to measure the iron-anomalous signal for single-wavelength anomalous dispersion phasing at 100 K.

Structure determination

Diffraction data were indexed, integrated, and scaled by XDS and XSCALE (67). The initial phases were obtained using SHELX C/D/E (68). The iron site identified was provided to the program SHARP/autoSHARP (69, 70) for density modification and automatic model building, which results in a model having 155 residues. The rest of the model was manually built with the program COOT (71, 72), and structural refinement was performed with the program Phenix (73). Ramachandran plot was calculated with the MolProbity (74). The statistics of data collection and structural refinement were summarized in Table 1. For prediction of the extra ligand in the Tll0287 protein, the software Arp/wARP (60) was used. The mF_o-DF_C map and 2mF_o-DF_c map without introducing any ligands were calculated using FFT in the CCP4 suite (75).

Homology search

Search of sequences homologous to Tll0287 was carried out with BLAST (76), and search of the three-dimensional structures similar to Tll0287 was performed by the DALI server (47). Superposition and RMSD calculation were performed by the LSQ Superpose function of Coot (71, 72) at the heme *c* ligand for comparison with that of PsbV2, and the SSM Superpose

function (77) for comparison with PAS-like domain proteins. Protein structure homology was also investigated with the Phyre[2] server (61).

MALDI-TOF mass analysis

To determine the molecular size of Tll0287, the sample was analyzed before the crystallization with MALDI-TOF/MS in linear mode (Voyager-DE PRO MALDI-TOF mass spectrometer; Applied Biosystems) as described previously (27). For identification of possible extra mass, the Tll0287 protein was digested with trypsin (Promega), and the polypeptides produced were analyzed with MALDI-TOF/MS in reflector mode after reduction and alkylation (78).

Prediction of the signal peptide and transmembrane helices

Possible peptide signal cleavage sites were predicted by the SignalP 4.1 Server (79), with the organism group set as Gram-negative bacteria. For prediction of the transmembrane helices, the HMMTOP server was used (80, 81).

Immunoblot analysis

Polyclonal antibodies against Tll0287 were obtained after several injections of purified Tll0287 (supplemental Fig. S5) into rabbits (Service de Pharmacologie et Immunoanalyse, iBiTec-S, CEA Saclay). Amersham Biosciences ELC Prime Western blotting detection reagents were used for immunoblot analysis (GE Healthcare). For the experiment in Fig. 1, whole cell samples were prepared by breaking the cell walls with lysozyme treatment as described previously (82, 83), and the resulting fraction was loaded onto SDS-polyacrylamide gel directly without separation of the soluble and membrane fractions. Thylakoid fractions and purified PsbA2-PSII core complexes were purified from the WT*2 strain as described previously (82, 84). For comparison, the Tll0287 protein purified from the WT*2 strain, whole cells, and thylakoid fractions of wild type expressing the *psbA1* gene predominately (WT) and those of a WT*3 (27) strain expressing the *psbA3* gene only were compared.

For determining the cellular location of Tll0287, thylakoid fraction of WT*2 were digested with a protease thermolysin (Sigma-Aldrich) at 5 μg protease/ml for 6 h at 25 °C, followed by detection with immunoblotting to determine the Tll0287 location. For comparison, the purified Tll0287 and PSII cores purified from the WT*2 strain was digested in the same way, and the PsbO protein was detected by immunoblotting with an anti-PsbO antibody from Agrisera (Vännäs, Sweden).

Electrochemistry

The redox potential of Tll0287 was determined with the same samples as that used for crystallization. Details of the thin-layer (6 μm) electrochemical cell used for the experiments are given in Ref. 85 except that the diamond windows were replaced by CaF_2 windows of 1-mm thickness. The working gold grid purchased from Euromip (France) was surface-modified by dipping it for 10 min into a 5 mM pyrimide-3-carboxyaldehyde thiosemicarbazone (Lancaster) solution heated to 80–90 °C, followed by careful washing of the gold grid with ultra-pure water. The following redox mediators (each at 40 μM final concentration) were used to accelerate the electrochemical reaction: methyl viologen (E_m = −440 mV *versus* NHE), benzyl viologen (E_m = −360 mV *versus* NHE), antraquinone 2-sulfonate (E_m = −225 mV *versus* NHE), 2 hydroxy 1–4 naphtoquinone (E_m = −128 mV *versus* NHE), 2,5-dihydroxy-*p*-benzoquinone (E_m = −62 mV *versus* NHE), duroquinone (−8 mV *versus* NHE), and phenazine ethosulfate (55 mV *versus* NHE).

Equilibrium redox titrations were performed by applying potentials to the working gold grid from −100 to −500 mV *versus* NHE with 20-mV intervals using a potentiostat (PRGE, Tacussel Electronique). For each potential step, the sample was allowed to equilibrate for 5 min. Spectra from 400 to 650 nm were recorded using a modified Cary 14 spectrophotometer equipped with a xenon light source and a UV-enhanced silicon detector. The data were analyzed by calculating the integrated Soret absorption (422–457 nm) obtained from the difference of the spectrum recorded at a given potential minus the spectrum of fully oxidized Tll0287 obtained at −100 mV *versus* NHE. The electrochemical cell was thermostatted at 15 °C with a water circulation system, and the sample compartment was purged with dry air.

Buffers at different pH values contained 200 mM NaCl, 0.03% β-DDM, and 50 mM of buffer MES, pH 5.5, 6.0, or 6.5; Tricine, pH 7.5; Tris, pH 8.5; or CAPS, pH 10.5. An aliquot of 9 μl of the Tll0287 sample solution adjusted to the buffer solution described above was mixed with 1 μl of mediator-buffer solution and dropped on the working gold grid. The path length of the closed electrochemical cell was adjusted to ~6 μm by adjusting the Amide I/H_2O absorption of the sample to ~0.8 using an FTIR spectrophotometer (Bruker Tensor 27).

Author contributions—J.-R. S. and A.B. conceived and coordinated the study. T. M. crystallized the protein; T. M. and M. Suga collected the X-ray diffraction data and analyzed the structure. A. N. and T. M. performed Western blot analysis, T. K. prepared the samples from the WT*2 strain, and M. Sugiura performed MS analysis. T.-L. L. and A. B. purified the protein; R. H. performed the redox analysis. W. N. performed the phylogenetic analysis, and T. M. performed structural homology analysis. T. M., M. Suga, W. N., A. B., and J.-R. S. wrote the manuscript, and all the authors reviewed the results and approved the final version of the manuscript.

Acknowledgments—We thank the staff members at Beamlines BL41XU and BL44XU of SPring-8 for help in data collection, the staff members of CCP4 structure solution workshop for prediction of the extra ligands, and Shinichiro Yonekura for help in performing the immunoblot analysis. Winfried Leibl, Anja Krieger, Frauke Baymann, Ghada Ajlani, Pierre Sétif, Alain Desbois, and Fabrice Rappaport are gratefully acknowledged for investment in some periods of this work and for helpful suggestions.

References

1. Umena, Y., Kawakami, K., Shen, J.-R., and Kamiya, N. (2011) Crystal structure of oxygen-evolving photosystem II at a resolution of 1.9 Å. *Nature* **473,** 55–60
2. Suga, M., Akita, F., Hirata, K., Ueno, G., Murakami, H., Nakajima, Y., Shimizu, T., Yamashita, K., Yamamoto, M., Ago, H., and Shen, J.-R. (2015) Native structure of photosystem II at 1.95 Å resolution viewed by femtosecond X-ray pulses. *Nature* **517,** 99–103

3. Wydrzynski, T. J., and Satoh, K. (eds.) (2005) *Photosystem II, the Light-Driven Water: Plastoquinone Oxidoreductase*, Springer, Dordrecht, The Netherlands
4. Shen, J.-R. (2015) Structure of Photosystem II and the mechanism of water oxidation in photosynthesis. *Annu. Rev. Plant Biol.* **66,** 23–48
5. Kawakami, K., Umena, Y., Kamiya, N., and Shen, J.-R. (2011) Structure of the catalytic, inorganic core of oxygen-evolving Photosystem II at 1.9 Å resolution. *J. Photochem. Photobiol. B* **104,** 9–18
6. Golden, S. S. (1995) Light-responsive gene expression in cyanobacteria. *J. Bacteriol.* **177,** 1651–1654
7. Schaefer, M. R., and Golden, S. (1989) Light availability influences the ratio of two forms of D1 in cyanobacterial thylakoids. *J. Biol. Chem.* **264,** 7412–7417
8. Schaefer, M. R., and Golden, S. S. (1989) Differential expression of members of a cyanobacterial psbA gene family in response to light. *J. Bacteriol.* **171,** 3973–3981
9. Bustos, S. A., Schaefer, M. R., and Golden, S. S. (1990) Different and rapid responses of four cyanobacterial *psbA* transcripts to changes in light intensity. *J. Bacteriol.* **172,** 1998–2004
10. Campbell, D., Eriksson, M.-J., Oquist G, Gustafsson, P., and Clarke, A. K. (1998) The cyanobacterium *Synechococcus* resists UV-B by exchanging photosystem II reaction-center D1 proteins. *Proc. Natl. Acad. Sci. U.S.A.* **95,** 364–369
11. Sicora, C. I., Appleton, S. E., Brown, C. M., Chung, J., Chandler, J., Cockshutt, A. M., Vass, I., and Campbell, D. A. (2006) Cyanobacterial *psbA* families in *Anabaena* and *Synechocystis* encode trace, constitutive and UVB-induced D1 isoforms. *Biochim. Biophys. Acta* **1757,** 47–56
12. Campbell, D., Zhou, G., Gustafsson, P., Oquist, G., and Clarke, A. K. (1995) Electron transport regulates exchange of two forms of photosystem II D1 protein in the cyanobacterium *Synechococcus*. *EMBO J.* **14,** 5457–5466
13. Sippola, K., and Aro, E.-M. (1999) Thiol redox state regulates expression of *psbA* genes in *Synechococcus* sp. PCC 7942. *Plant Mol. Biol.* **41,** 425–433
14. Summerfield, T. C., Toepel, J., and Sherman, L. A. (2008) Low-oxygen induction of normally cryptic *psbA* genes in cyanobacteria. *Biochemistry* **47,** 12939–12941
15. Sicora, C. I., Ho, F. M., Salminen, T., Styring, S., and Aro, E.-M. (2009) Transcription of a "silent" cyanobacterial *psbA* gene is induced by microaerobic conditions. *Biochim. Biophys. Acta* **1787,** 105–112
16. Mulo, P., Sicora, C., and Aro, E.-M. (2009) Cyanobacterial *psbA* gene family: optimization of oxygenic photosynthesis. *Cell Mol. Life Sci.* **66,** 3697–3710
17. Nakamura, Y., Kaneko, T., Sato, S., Ikeuchi, M., Katoh, H., Sasamoto, S., Watanabe, A., Iriguchi, M., Kawashima, K., Kimura, T., Kishida, Y., Kiyokawa, C., Kohara, M., Matsumoto, M., Matsuno, A., *et al.* (2002) Complete genome structure of the thermophilic cyanobacterium *Thermosynechococcus elongatus* BP-1. *DNA Res.* **9,** 123–130
18. Kós, P. B., Deák, Z., Cheregi, O., and Vass, I. (2008) Differential regulation of *psbA* and *psbD* gene expression, and the role of the different D1 protein copies in the cyanobacterium *Thermosynechococcus elongatus* BP-1. *Biochim. Biophys. Acta* **1777,** 74–83
19. Sander, J., Nowaczyk, M., Kopczak, M., and Rögner, M. (2008) Role of the *psbA* gene family of PSII from the thermophilic cyanobacterium *Thermosynechococcus elongatus.* In *Photosynthesis: Energy from the Sun*, pp. 745–748, Springer-Verlag, New York Inc., New York
20. Sugiura, M., and Boussac, A. (2014) Some Photosystem II properties depending on the D1 protein variants in *Thermosynechococcus elongatus*. *Biochim. Biophys. Acta* **1837,** 1427–1434
21. Sugiura, M., and Boussac, A. (2014) Photosystem II D1 protein variants in *Thermosynechococcus elongatus*. *Res. Chem. Intermed.* **40,** 3219–3229
22. Sugiura, M., Ogami, S., Kusumi, M., Un, S., Rappaport, F., and Boussac, A. (2012) Environment of TyrZ in Photosystem II from *Thermosynechococcus elongatus* in which PsbA2 is the D1 protein. *J. Biol. Chem.* **287,** 13336–13347
23. Sugiura, M., Boussac, A., Noguchi, T., and Rappaport, F. (2008) Influence of histidine-198 of the D1 subunit on the properties of the primary electron donor, P 680, of photosystem II in *Thermosynechococcus elongatus*. *Biochim. Biophys. Acta* **1777,** 331–342
24. Sugiura, M., Ozaki, Y., Nakamura, M., Cox, N., Rappaport, F., and Boussac, A. (2014) The D1–173 amino acid is a structural determinant of the critical interaction between D1-Tyr161 (Tyr Z) and D1-His190 in Photosystem II. *Biochim. Biophys. Acta* **1837,** 1922–1931
25. Sugiura, M., Kato, Y., Takahashi, R., Suzuki, H., Watanabe, T., Noguchi, T., Rappaport, F., and Boussac, A. (2010) Energetics in Photosystem II from *Thermosynechococcus elongatus* with a D1 protein encoded by either the *psbA1* or *psbA3* gene. *Biochim. Biophys. Acta* **1797,** 1491–1499
26. Boussac, A., Sugiura, M., and Rappaport, F. (2011) Probing the quinone binding site of Photosystem II from *Thermosynechococcus elongatus* containing either PsbA1 or PsbA3 as the D1 protein through the binding characteristics of herbicides. *Biochim. Biophys. Acta* **1807,** 119–129
27. Boussac, A., Koyama, K., and Sugiura, M. (2013) The Tll0287 protein is a hemoprotein associated with the PsbA2-Photosystem II complex in *Thermosynechococcus elongatus*. *Biochim. Biophys. Acta* **1827,** 1174–1182
28. Dutton, P. L. (1978) Redox potentiometry: determination of midpoint potentials of oxidation-reduction components of biological electron-transfer systems. *Methods Enzymol.* **54,** 411–435
29. Mitschke, J., Georg, J., Scholz, I., Sharma, C. M., Dienst, D., Bantscheff, J., Voss, B., Steglich, C., Wilde, A., Vogel, J., and Hess, W. R. (2011) An experimentally anchored map of transcriptional start sites in the model cyanobacterium *Synechocystis sp.* PCC6803. *Proc. Natl. Acad. Sci. U.S.A.* **108,** 2124–2129
30. Kerfeld, C. A., Yoshida, S., Tran, K. T., Yeates, T. O., Cascio, D., Bottin, H., Berthomieu, C., Sugiura, M., and Boussac, A. (2003) The 1.6 Å resolution structure of Fe-superoxide dismutase from the thermophilic cyanobacterium *Thermosynechococcus elongatus*. *J. Biol. Inorg. Chem.* **8,** 707–714
31. Kerfeld, C. A., Sawaya, M. R., Bottin, H., Tran, K. T., Sugiura, M., Cascio, D., Desbois, A., Yeates, T. O., Kirilovsky, D., and Boussac, A. (2003) Structural and EPR Characterization of the soluble form of cytochrome *c*-550 and of the psbV2 gene product from the cyanobacterium *Thermosynechococcus elongatus*. *Plant Cell Physiol.* **44,** 697–706
32. Grein, F., Venceslau, S. S., Schneider, L., Hildebrandt, P., Todorovic, S., Pereira, I. A., and Dahl, C. (2010) DsrJ, an essential part of the DsrMKJOP transmembrane complex in the purple sulfur bacterium *Allochromatium vinosum*, is an unusual trihem cytochrome *c*. *Biochemistry* **49,** 8290–8299
33. Ukita, S., Fujii, T., Hira, D., Nishiyama, T., Kawase, T., Migita, C. T., and Furukawa, K. (2010) Heterodimeric cytochrome *c* complex with a very low redox potential from an anaerobic ammonium-oxidizing enrichment culture. *FEMS Microbiol. Lett.* **313,** 61–67
34. Kappler, U., and Maher, M. J. (2013) The bacterial SoxAX cytochromes. *Cell. Mol. Life Sci.* **70,** 977–992
35. Alric, J., Tsukatani, Y., Yoshida, M., Matsuura, K., Shimada, K., Hienerwadel, R., Schoepp-Cothenet, B., Nitschke, W., Nagashima, K. V., and Verméglio, A. (2004) Structural and functional characterization of the unusual triheme cytochrome bound to the reaction center of *Rhodovulum sulfidophilum*. *J. Biol. Chem.* **279,** 26090–26097
36. Van Driessche, G., Devreese, B., Fitch, J. C., Meyer, T. E., Cusanovich, M. A., and Van Beeumen, J. J. (2006) GHP, a new c-type green heme protein from *Halobacterium salexigens* and other proteobacteria. *FEBS J.* **273,** 2801–2811
37. Suga, M., Lai, T.-L., Sugiura, M., Shen, J.-R., and Boussac, A. (2013) Crystal structure at 1.5 Å resolution of the PsbV2 cytochrome from the cyanobacterium *Thermosynechococcus elongatus*. *FEBS Lett.* **587,** 3267–3272
38. Katoh, H., Itoh, S., Shen, J.-R., and Ikeuchi, M. (2001) Functional analysis of *psbV* and a novel c-type cytochrome gene *psbV2* of the thermophilic cyanobacterium *Thermosynechococcus elongatus* strain BP-1. *Plant Cell Physiol.* **42,** 599–607
39. Peisach, J., Blumberg, W. E., and Adler, A. (1973) Electron paramagnetic resonance studies of iron porphyrin and chlorin systems. *Ann. N.Y. Acad. Sci.* **206,** 310–327

40. Walker, F. A. (1999) Magnetic spectroscopic (EPR, ESEEM, Mossbauer, MCD and NMR) studies of low-spin ferriheme centers and their corresponding heme proteins. *Coord. Chem. Rev.* **186,** 471–534
41. Meier, M., Janosik, M., Kery, V., Kraus, J. P., and Burkhard, P. (2001) Structure of human cystathionine β-synthase: a unique pyridoxal 5′-phosphate-dependent heme protein. *EMBO J.* **20,** 3910–3916
42. Burton, M. J., Kapetanaki, S. M., Chernova, T., Jamieson, A. G., Dorlet, P., Santolini, J., Moody, P. C., Mitcheson, J. S., Davies, N. W., Schmid, R., Raven, E. L., and Storey, N. M. (2016) A heme-binding domain controls regulation of ATP-dependent potassium channels. *Proc. Natl. Acad. Sci. U.S.A.* **113,** 3785–3790
43. Díaz-Moreno, I., Hulsker, R., Skubak, P., Foerster, J. M., Cavazzini, D., Finiguerra, M. G., Díaz-Quintana, A., Moreno-Beltrán, B., Rossi, G. L., Ullmann, G. M., Pannu, N. S., De la Rosa, M. A., and Ubbink, M. (2014) The dynamic complex of cytochrome c_6 and cytochrome f studied with paramagnetic NMR spectroscopy. *Biochim. Biophys. Acta* **1837,** 1305–1315
44. Smith, A. T., Marvin, K. A., Freeman, K. M., Kerby, R. L., Roberts, G. P., and Burstyn, J. N. (2012) Identification of Cys94 as the distal ligand to the Fe(III) heme in the transcriptional regulator RcoM-2 from *Burkholderia xenovorans*. *J. Biol. Inorg. Chem.* **17,** 1071–1082
45. Zhong, F., Lisi, G. P., Collins, D. P., Dawson, J. H., and Pletneva, E. V. (2014) Redox-dependent stability, protonation, and reactivity of cysteine-bound heme proteins. *Proc. Natl. Acad. Sci. U.S.A.* **111,** E306–E315
46. Kirilovsky, D., Roncel, M., Boussac, A., Wilson, A., Zurita, J.-L., Ducruet, J.-M., Bottin, H., Sugiura, M., Ortega, J.-M., and Rutherford, A. W. (2004) Cytochrome c_{550} in the cyanobacterium *Thermosynechococcus elongatus*: study of redox mutants. *J. Biol. Chem.* **279,** 52869–52880
47. Holm, L., and Rosenström, P. (2010) DALI server: conservation mapping in 3D. *Nucleic Acids Res.* **38,** W545–W549
48. Wu, R., Gu, M., Wilton, R., Babnigg, G., Kim, Y., Pokkuluri, P. R., Szurmant, H., Joachimiak, A., and Schiffer, M. (2013) Insight into the sporulation phosphorelay: crystal structure of the sensor domain of *Bacillus subtilis* histidine kinase, KinD. *Protein Sci.* **22,** 564–576
49. Cheung, J., and Hendrickson, W. A. (2010) Sensor domains of two-component regulatory systems. *Curr. Opin. Microbiol.* **13,** 116–123
50. Hoffman, E. C., Reyes, H., Chu, F.-F., Sander, F., Conley, L. H., Brooks, B. A., and Hankinson, O. (1991) Cloning of a factor required for activity of the Ah (dioxin) receptor. *Science* **252,** 954–958
51. Nambu, J. R., Lewis, J. O., Wharton, K. A., Jr., and Crews, S. T. (1991) The *Drosophila* single-minded gene encodes a helix-loop-helix protein that acts as a master regulator of CNS midline development. *Cell* **67,** 1157–1167
52. Dunlap, J. C. (1996) Genetic and molecular analysis of circadian rhythms. *Ann. Rev. Genet.* **30,** 579–601
53. Taylor, B. L., and Zhulin, I. B. (1999) PAS domains: internal sensors of oxygen, redox potential, and light. *Microb. Mol. Biol. Rev.* **63,** 479–506
54. Crosthwaite, S. K., Dunlap, J. C., and Loros, J. J. (1997) Neurospora *wc-1* and *wc-2*: transcription, photoresponses, and the origins of circadian rhythmicity. *Science* **276,** 763–769
55. Morais Cabral, J. H., Lee, A., Cohen, S. L., Chait, B. T., Li, M., and Mackinnon, R. (1998) Crystal structure and functional analysis of the HERG potassium channel N terminus: a eukaryotic PAS domain. *Cell* **95,** 649–655
56. Möglich, A., Ayers, R. A., and Moffat, K. (2009) Structure and signaling mechanism of Per-Arnt-Sim domains. *Structure* **17,** 1282–1294
57. Henry, J. T., and Crosson, S. (2011) Ligand binding PAS domains in a genomic, cellular, and structural context. *Annu. Rev. Microbiol.* **65,** 261–286
58. Kneuper, H., Scheu, P., Etzkorn, M., Sevvana, M., Dünnwald, P., Becker, S., Baldus, M., Griesinger, C., and Unden, G. (2010) Sensing ligands by periplasmic sensing histidine kinases with sensory PAS domains. In *Sensory Mechanisms in Bacteria: Molecular Aspects of Signal Recognition* (Spiro, S., and Dixon, R., eds) Caister Academic Press, Poole, UK
59. Glekas, G. D., Mulhern, B. J., Kroc, A., Duelfer, K. A., Lei, V., Rao, C. V., and Ordal, G. W. (2012) The *Bacillus subtilis* chemoreceptor McpC senses multiple ligands using two discrete mechanisms. *J. Biol. Chem.* **287,** 39412–39418
60. Langer, G., Cohen, S. X., Lamzin, V. S., and Perrakis, A. (2008) Automated macromolecular model building for X-ray crystallography using ARP/wARP version 7. *Nat. Protoc.* **3,** 1171–1179
61. Kelley, L. A., Mezulis, S., Yates, C. M., Wass, M. N., and Sternberg, M. J. (2015) The Phyre^2 web portal for protein modeling, prediction and analysis. *Nat. Protoc.* **10,** 845–858
62. Pokkuluri, P. R., Pessanha, M., Londer, Y. Y., Wood, S. J., Duke, N. E., Wilton, R., Catarino, T., Salgueiro, C. A., and Schiffer, M. (2008) Structures and solution properties of two novel periplasmic sensor domains with *c*-type heme from chemotaxis proteins of *Geobacter sulfurreducens*: implications for signal transduction. *J. Mol. Biol.* **377,** 1498–1517
63. Arieli, B., Shahak, Y., Taglicht, D., Hauska, G., and Padan, E. (1994) Purification and characterisation of sulfide-quinone reductase, a novel enzyme driving anoxygenic photosynthesis in *Oscillatoria limnetica*. *J. Biol. Chem.* **269,** 5705–5711
64. Hirano, Y., Kimura, Y., Suzuki, H., Miki, K., and Wang, Z. Y. (2012) Structure analysis and comparative characterization of the cytochrome *c*′ and flavocytochrome *c* from thermophilic purple photosynthetic bacterium *Thermochromatium tepidum*. *Biochemistry* **51,** 6556–6567
65. Touw, W. G., Baakman, C., Black, J., te Beek, T. A., Krieger, E., Joosten, R. P., and Vriend, G. (2015) A series of PDB-related databanks for everyday needs. *Nucleic Acids Res.* **43,** D364–D368
66. Kabsch, W., and Sander, C. (1983) Dictionary of protein secondary structure: pattern recognition of hydrogen-bonded and geometrical features. *Biopolymers* **22,** 2577–2637
67. Kabsch, W. (2010) XDS. *Acta Crystallogr. D* **66,** 125–132
68. Sheldrick, G. M. (2010) Experimental phasing with SHELXC/D/E: combining chain tracing with density modification. *Acta Crystallogr. D* **66,** 479–485
69. Bricogne, G., Vonrhein, C., Flensburg, C., Schiltz, M., and Paciorek, W. (2003) Generation, representation and flow of phase information in structure determination: recent developments in and around SHARP 2.0. *Acta Crystallogr. D* **59,** 2023–2030
70. Vonrhein, C., Blanc, E., Roversi, P., and Bricogne, G. (2007) Automated structure solution with autoSHARP. In *Macromolecular Crystallography Protocols*, pp 215–230, Springer-Verlag, New York Inc., New York
71. Emsley, P., and Cowtan, K. (2004) Coot: model-building tools for molecular graphics. *Acta Crystallogr. D* **60,** 2126–2132
72. Emsley, P., Lohkamp, B., Scott, W. G., and Cowtan, K. (2010) Features and development of Coot. *Acta Crystallogr. D* **66,** 486–501
73. Adams, P. D., Afonine, P. V., Bunkóczi, G., Chen, V. B., Davis, I. W., Echols, N., Headd, J. J., Hung, L.-W., Kapral, G. J., Grosse-Kunstleve, R. W., McCoy, A. J., Moriarty, N. W., Oeffner, R., Read, R. J., Richardson, D. C., *et al.* (2010) PHENIX: a comprehensive Python-based system for macromolecular structure solution. *Acta Crystallogr. D* **66,** 213–221
74. Chen, V. B., Arendall, W. B., 3rd, Headd, J. J., Keedy, D. A., Immormino, R. M., Kapral, G. J., Murray, L. W., Richardson, J. S., and Richardson, D. C. (2010) MolProbity: all-atom structure validation for macromolecular crystallography. *Acta Crystallogr. D* **66,** 12–21
75. Winn, M. D., Ballard, C. C., Cowtan, K. D., Dodson, E. J., Emsley, P., Evans, P. R., Keegan, R. M., Krissinel, E. B., Leslie, A. G., McCoy, A., McNicholas, S. J., Murshudov, G. N., Pannu, N. S., Potterton, E. A., Powell, H. R., *et al.* (2011) Overview of the CCP4 suite and current developments. *Acta Crystallogr. D* **67,** 235–242
76. Altschul, S. F., Madden, T. L., Schäffer, A. A., Zhang, J., Zhang, Z., Miller, W., and Lipman, D. J. (1997) Gapped BLAST and PSI-BLAST: a new generation of protein database search programs. *Nucleic Acids Res.* **25,** 3389–3402
77. Krissinel, E., and Henrick, K. (2004) Secondary-structure matching (SSM), a new tool for fast protein structure alignment in three dimensions. *Acta Crystallogr. D* **60,** 2256–2268
78. Sugiura, M., Koyama, K., Umena, Y., Kawakami, K., Shen, J.-R., Kamiya, N., and Boussac, A. (2013) Evidence for an unprecedented histidine hydroxyl modification on D2-His336 in Photosystem II of *Thermosynechoc-*

cocus vulcanus and *Thermosynechoccocus elongatus*. *Biochemistry* **52,** 9426–9431
79. Petersen, T. N., Brunak, S., von Heijne, G., and Nielsen, H. (2011) SignalP 4.0: discriminating signal peptides from transmembrane regions. *Nat. Methods* **8,** 785–786
80. Tusnády, G. E., and Simon, I. (1998) Principles governing amino acid composition of integral membrane proteins: application to topology prediction. *J. Mol. Biol.* **283,** 489–506
81. Tusnády, G. E., and Simon, I. (2001) The HMMTOP transmembrane topology prediction server. *Bioinformatics* **17,** 849–850
82. Shen, J.-R., and Inoue, Y. (1993) Binding and functional properties of two new extrinsic components, cytochrome *c*-550 and a 12-kDa protein, in cyanobacterial photosystem II. *Biochemistry* **32,** 1825–1832
83. Shen, J.-R., and Kamiya, N. (2000) Crystallization and the crystal properties of the oxygen-evolving photosystem II from *Synechococcus vulcanus*. *Biochemistry* **39,** 14739–14744
84. Shen, J.-R., and Inoue, Y. (1993) Cellular localization of cytochrome *c*-550: its specific association with cyanobacterial photosystem II. *J. Biol. Chem.* **268,** 20408–20413
85. Vita, N., Brubach, J.-B., Hienerwadel, R., Bremond, N., Berthomieu, D., Roy and P., Berthomieu, C. (2013) Electrochemically induced far-infrared difference spectroscopy on metalloproteins using advanced synchrotron technology. *Anal. Chem.* **85,** 2891–2898

Crystal structure and redox properties of a novel cyanobacterial heme protein with a His/Cys heme axial ligation and a Per-Arnt-Sim (PAS)-like domain

Taiki Motomura, Michihiro Suga, Rainer Hienerwadel, Akiko Nakagawa, Thanh-Lan Lai, Wolfgang Nitschke, Takahiro Kuma, Miwa Sugiura, Alain Boussac and Jian-Ren Shen

J. Biol. Chem. 2017, 292:9599-9612.
doi: 10.1074/jbc.M116.746263 originally published online April 20, 2017